# A SEARCH FOR THE SUPERSYMMETRIC PARTNER OF THE $Z^0$ IN $e^+e^-$ ANNIHILATION AT PETRA

JADE Collaboration

W. BARTEL, L. BECKER, C. BOWDERY [1], D. CORDS [2], R. FELST, D. HAIDT, H. JUNGE [3], G. KNIES, H. KREHBIEL, P. LAURIKAINEN [4], R. MEINKE, B. NAROSKA, J. OLSSON, E. PIETARINEN [4], D. SCHMIDT [3], P. STEFFEN, M. ZACHARA
*Deutsches Elektronen-Synchrotron DESY, Hamburg, Germany*

G. DIETRICH, E. ELSEN [2], G. HEINZELMANN, H. KADO, M. KUHLEN, T. MASHIMO, K. MEIER, A. PETERSEN, U. SCHNEEKLOTH, G. WEBER
*II. Institut für Experimentalphysik der Universität Hamburg, Germany*

K. AMBRUS, S. BETHKE, A. DIECKMANN, J. HEINTZE, K.H. HELLENBRAND, R.D. HEUER [5], S. KOMAMIYA, J. von KROGH, P. LENNERT, H. MATSUMURA, H. RIESEBERG, J. SPITZER, A. WAGNER
*Physikalisches Institut der Universität Heidelberg, Germany*

A. FINCH, F. FOSTER, G. HUGHES, T. NOZAKI [6], J. NYE
*University of Lancaster, England*

J. ALLISON, J. BAINES, A.H. BALL, R.J. BARLOW, J. CHRIN, I.P. DUERDOTH, T. GREENSHAW, P. HILL, F.K. LOEBINGER, A.A. MACBETH, H. McCANN, H.E. MILLS, P.G. MURPHY, K. STEPHENS, P. WARMING
*University of Manchester, England*

R.G. GLASSER, B. SECHI-ZORN, J.A.J. SKARD, S.R. WAGNER, G.T. ZORN
*University of Maryland [7], MD, USA*

S.L. CARTWRIGHT, D. CLARKE, R. MARSHALL, R. MIDDLETON, J.B. WHITTAKER
*Rutherford Appleton Laboratory, Chilton, England*

and

J. KANZAKI, T. KAWAMOTO, T. KOBAYASHI, M. KOSHIBA, M. MINOWA, M. NOZAKI, S. ORITO, A. SATO, H. TAKEDA, T. TAKESHITA, Y. TOTSUKA and S. YAMADA
*Laboratory of International Collaboration on Elementary Particle Physics and Department of Physics, University of Tokyo, Japan*

Received 15 August 1984

[1] European Science Exchange Fellow.
[2] Present address: SLAC, CA, USA.
[3] Universität Gesamthochschule Wuppertal, Germany.
[4] University Helsinki, Helsinki, Finland.
[5] Present address: CERN, Geneva, Switzerland.
[6] Present address: KEK, Ibaraki, Japan.
[7] Partially supported by Department of Energy, USA.



0370-2693/84/$03.00 © Elsevier Science Publishers B.V. (North-Holland Physics Publishing Division)

A search has been made for the zino $\tilde{Z}$, the supersymmetric partner of the $Z^0$, in $e^+e^-$ annihilation at PETRA using the JADE detector. In supersymmetric theories the zino is produced together with a photino ($e^+e^- \to \tilde{Z}\tilde{\gamma}$), by an exchange of a scalar electron $\tilde{e}$. The $\tilde{Z}$ decay modes investigated are $e^+e^-\tilde{\gamma}$, $\mu^+\mu^-\tilde{\gamma}$, $q\bar{q}\tilde{\gamma}$ and $q\bar{q}\tilde{g}$ (with subsequent gluino decay $\tilde{g} \to q\bar{q}\tilde{\gamma}$) No evidence for these events has been observed. Limits are presented as a function of $\tilde{Z}$ mass, $\tilde{\gamma}$ mass and $\tilde{e}$ mass.

In supersymmetric theories, each elementary particle has a supersymmetric partner whose spin differs by 1/2 from that of the particle [1]. The supersymmetric partner of the weak intermediate vector boson $Z^0$ is called the zino $\tilde{Z}$ and is a spin 1/2 fermion [‡1]. It interacts with an ordinary fermion (lepton or quark) and its supersymmetric partner (scalar lepton or scalar quark). Limits from the JADE experiment on other supersymmetric particles are given elsewhere [3]. In several supersymmetric theories, the zino mass is expected to be smaller than the $Z^0$ mass [4]. The most promising way to look for the zino is to study its single production in $e^+e^-$ annihilation, accompanied by a photino $\tilde{\gamma}$ ($e^+e^- \to \tilde{Z}\tilde{\gamma}$). It is produced by an exchange of a scalar electron $\tilde{e}$ as shown in fig. 1a. If the photino is lighter than the zino, as generally expected, this channel opens before the pair production channel ($e^+e^- \to \tilde{Z}\tilde{Z}$). These processes are similar to two-photino production ($e^+e^- \to \tilde{\gamma}\tilde{\gamma}$) with one or both photinos replaced by zinos. In this analysis we assume that the photino is stable as expected in most local supersymmetric theories. We also assume that the supersymmetric partners of left-handed and right-handed electrons, $\tilde{e}_L$ and $\tilde{e}_R$, have equal mass [5].

The zino can decay either into a lepton pair plus a photino ($\ell\bar{\ell}\tilde{\gamma}$), a quark pair plus a photino ($q\bar{q}\tilde{\gamma}$) or into a quark pair plus a gluino ($q\bar{q}\tilde{g}$) via a real or a virtual corresponding supersymmetric partner (scalar lepton $\tilde{\ell}$ or scalar quark $\tilde{q}$) [‡2]. If the zino is light enough so that it can be produced at PETRA, its decay would most probably be via virtual states of $\tilde{\ell}$ or $\tilde{q}$. If all $\tilde{\ell}$'s and $\tilde{q}$'s have similar masses and the gluino mass is small, the channel $\tilde{Z} \to q\bar{q}\tilde{g}$ is dominant because of the large strong coupling constant relative to the electromagnetic one. In this analysis [‡3] we have

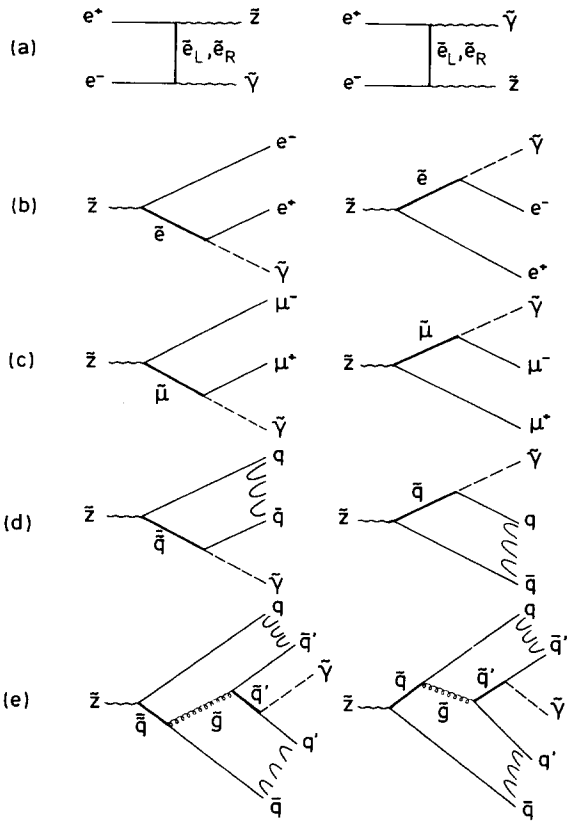


Fig. 1. Diagrams for zino production and decay. (a) Single zino production together with a photino in $e^+e^-$ annihilation by the exchange of a scalar electron. (b) Leptonic decay of zino into $e^+e^-\tilde{\gamma}$. (c) Leptonic decay of zino into $\mu^+\mu^-\tilde{\gamma}$. (d) Hadronic decay of zino into $q\bar{q}\tilde{\gamma}$, with subsequent fragmentation between q and between $\bar{q}$. (e) Hadronic decay of zino into $q\bar{q}\tilde{g}$, with sequential decay of $\tilde{g}$ into $q'\bar{q}'\tilde{\gamma}$. The fragmentation takes place between $q'\bar{q}$ and $q\bar{q}'$.

[‡1] In general, the mass eigenstates could be a mixture of photino, zino and neutral higgsinos [2]. For simplicity and definiteness, we do not consider such mixing.

[‡2] If the scalar neutrinos $\tilde{\nu}$ are very much lighter than other scalar leptons or scalar quarks, the dominant decay mode would be $\tilde{\nu}\bar{\nu}$ or $\bar{\tilde{\nu}}\nu$. With the $\tilde{\nu}$'s unobservable, it would be very difficult to detect the zino in this case. The zino lifetime is predicted to be typically shorter than $10^{-12}$ s [6]. If the zino is very light ($\lesssim$2 GeV) and all the scalars ($\tilde{\ell}$, $\tilde{\nu}$ and $\tilde{q}$ are heavy ($\gtrsim$100 GeV) and the gluino is heavy as well ($\gtrsim M(\tilde{Z})$), the life time would be of the order of $10^{-11}$ s, which is still acceptable for our search.

[‡3] Because of the improved cuts and the higher luminosity used in this analysis, improved limits are obtained as compared to those given in ref. [7].

studied the following 4 processes (see fig. 1b–1e)

process (1):

$e^+e^- \to \tilde{Z}\tilde{\gamma}, \quad \tilde{Z} \to e^+e^-\tilde{\gamma}$ ,

process (2):

$e^+e^- \to \tilde{Z}\tilde{\gamma}, \quad \tilde{Z} \to \mu^+\mu^-\tilde{\gamma}$ ,

process (3):

$e^+e^- \to \tilde{Z}\tilde{\gamma}, \quad \tilde{Z} \to q\bar{q}\tilde{\gamma}$ ,

process (4):

$e^+e^- \to \tilde{Z}\tilde{\gamma}, \quad \tilde{Z} \to q\bar{q}\tilde{g}, \quad \tilde{g} \to q'\bar{q}'\tilde{\gamma}$ .

The photino escapes undetected, almost like a neutrino [‡4]. Since there are two invisible photinos in these reactions, their distinctive feature is a large missing momentum and a large acoplanarity. Our analysis is based on this. The selection cuts and the detection efficiencies were determined with Monte Carlo calculations in which the production and the decay was simulated with detector effects included. Radiative corrections were not applied because they have uncertainties due to the existence of supersymmetric particles. For zino production, we used the differential cross section as given by Reya [9]. The total cross section for single zino production depends on the scalar electron mass, zino mass and $\sqrt{s}$. If the scalar electron mass is less than 100 GeV and both $\tilde{Z}$ and $\tilde{\gamma}$ are light ($M(\tilde{Z}) + M(\tilde{\gamma}) < E_{\text{beam}}$), the total cross section is of the order of 0.1–40 pb at CM energy of 35 GeV [6,9], which is large enough for detection if the events have distinctive features. The matrix elements for zino and gluino decay were calculated by Reiter et al. [10]. For the fragmentation of quarks, the Lund string model [11] was used. The parameters in the model had been optimized using multihadron data [12]. The application of the Lund model to the process (3) is unique and straightforward (see fig. 1d), i.e. the colour string is stretched between the q and $\bar{q}$. For the process (4), there are two colour singlet strings stretched between q and $\bar{q}'$ and between q′ and $\bar{q}$. The fragmentation takes place within these strings (see fig. 1e) [‡5].

The data analysis is based on an integrated luminosity of 74 $pb^{-1}$ in the CM energy range 27–37 GeV accumulated from summer 1979 to summer 1982 and 14 $pb^{-1}$ in the CM energy range 37–46 GeV accumulated from autumn 1982 to spring 1984. The details of the JADE detector and the trigger conditions are described elsewhere [13,14].

In the following we discuss the search for reactions (1)–(4) separately, since the selection criteria differ from case to case.

*Case (A).* $\tilde{Z} \to e^+e^-\tilde{\gamma}$. The selection criteria used are described below. Note that they are identical to those used in our search for $e^+e^- \to \tilde{e}^+\tilde{e}^-$ or $e\tilde{e}\tilde{\gamma}$ discussed elsewhere [‡6]. For sufficiently large zino masses, the angle between the decay electrons is large enough to result in two separate clusters in the lead-glass. For low zino masses, however, the electrons are emitted into a narrow cone so that the lead-glass clusters overlap and cannot be resolved into two. For this reason, the search is made both for events with two acoplanar energy clusters (criteria (A1)) as well as for events with only one lead-glass cluster (criteria (A2)).

(A1) Selection of events with two acoplanar clusters.

(1) At least two lead-glass clusters were required with an energy larger than $E_{\text{beam}}/4$ and $|\cos\vartheta| < 0.75$, where $\vartheta$ is the polar angle relative to the positron beam axis.

(2) The total energy for all the other clusters had to be less than 1 GeV.

(3) Each of the two high energy clusters had to be associated with one or more charged tracks in the central detector in order to include showering electrons. Furthermore no charged tracks with $p > 0.2$ GeV/$c$ were allowed outside a 10° cone around the cluster direction.

‡4 The interaction cross section of photinos is predicted to be very small. Even the process $\tilde{\gamma}q \to \tilde{g}q$ has the extremely small cross section of $< 2 \times 10^{-32}$ cm$^2$ for $E(\tilde{\gamma}) < E_{\text{beam}}$, $M(\tilde{\gamma}) = 0$ GeV and $M(\tilde{q}) > 10$ GeV [8].

‡5 As discussed in the text, the fragmentation in the model calculation was applied along colour strings between the final quarks and antiquarks, i.e. after the decay of the $\tilde{q}$ or the $\tilde{g}$. Actually, if the $\tilde{q}$ in reaction (3) is on the mass shell the fragmentation starts between the $\tilde{q}$ and the antiquark. The $\tilde{q}$ would then be part of a hadron before it decays into $q\tilde{\gamma}$. The situation is similar for reaction (4). There the $\tilde{g}$ fragments, before it decays, along two colour strips between $\tilde{g}\bar{q}$ and $\tilde{g}q$, respectively. The colour singlet bound state containing the $\tilde{g}$ then decays. The detection efficiencies should not differ very much from that for the simple scheme adopted by us since the photino produced together with the zino carries a large percentage of the total energy.

‡6 For a search for supersymmetric partner of electrons, see ref. [15].

(4) The acoplanarity angles for the two lead-glass clusters had to satisfy $\varphi_{\text{acop}} > 40°$, where $\cos\varphi_{\text{acop}} = -(\boldsymbol{p}_1 \times \hat{z})\cdot(\boldsymbol{p}_2 \times \hat{z})/(|\boldsymbol{p}_1 \times \hat{z}|\cdot|\boldsymbol{p}_2 \times \hat{z}|)$. $\boldsymbol{p}_1$ and $\boldsymbol{p}_2$ are the momentum vectors of the two clusters and $\hat{z}$ is a unit vector in the positron beam direction.

(5) Events with small missing masses were rejected when the direction of the missing momentum was close to the beam axis: i.e. events with $|(\text{missing mass})^2| < 70\ \text{GeV}^2$ and $|\cos\vartheta_{\text{miss}}| > 0.7$ were rejected, where $\vartheta_{\text{miss}}$ is the polar angle of the total missing momentum.

(6) In order to reject two photon events $e^+e^- \to e^+e^-e^+e^-$, events were rejected if the forward tagging counters had energy deposits. In order to reject $e^+e^-\gamma$ events with the $\gamma$ escaping through small gaps between the lead-glass blocks [‡7], events were rejected if the innermost muon chambers or forward muon counters exhibited hits behind a gap consistent with hits due to an electromagnetic shower.

(A2) Selection of events with a single high energy cluster.

(1) One lead-glass cluster was required with $E > E_{\text{beam}}/4$ and $|\cos\vartheta| < 0.75$.

(2) The total energy for all the other clusters had to be less than 1 GeV.

(3) The cluster had to be associated with one or more charged tracks with $p > 0.2$ GeV/$c$. No charged tracks were allowed outside a 10° cone around the cluster direction.

(4) The cluster had to have transverse energy with respect to the beam axis greater than $0.65\,E_{\text{beam}}$.

(5) Cuts (1)–(4) can be satisfied by events $e^+e^- \to \gamma\gamma$ with one photon converting in the beam pipe and the opposite photon escaping through small gaps between the lead-glass blocks. To take this into account, events were rejected if the innermost muon chambers within ±10° opposite to the electron candidate exhibited hits which were consistent with hits due to an electromagnetic shower.

For both selections (A1) and (A2), no events survived after the cuts. A combined detection efficiency for either cut (A1) or (A2) was then determined by Monte Carlo calculation as a function of $\tilde{\gamma}$-, $\tilde{e}$- and $\tilde{Z}$-mass. As an example, we give here its dependence on the zino mass for the case of massless photinos and $M(\tilde{e}) = 50$ GeV. The efficiency rises from about 15% at $M(\tilde{Z}) = 5$ GeV to about 25% at $M(\tilde{Z}) = 25$ GeV. Above this point it stays approximately constant. The efficiency varies very slowly with the $\tilde{e}$ mass.

Lower limits for $M(\tilde{Z})$ and $M(\tilde{e})$ can now be obtained by comparing the observed number of events with the expected number $N_{\text{prod}}\epsilon\cdot\text{Br}(\tilde{Z} \to e^+e^-\tilde{\gamma})$. Here $N_{\text{prod}}$ is the total number of events expected, given by the theoretical cross section and the experimental luminosity at various values of $\sqrt{s}$, $\epsilon$ is the averaged detection efficiency for these events, and Br is the $\tilde{Z}$ decay branching ratio. The branching ratio can, in principle, be calculated as a function of the masses. It depends, however, on the full mass spectrum, both of the ordinary and supersymmetric particles. For this reason we chose to take the branching ratio as a free parameter in the lower limit calculation. For $M(\tilde{Z})$, $M(\tilde{\gamma})$ and $M(\tilde{e})$ fixed, the limit on Br can then be obtained from

$$\text{Br}(\tilde{Z} \to e^+e^-\tilde{\gamma}) < N_{\text{obs}}(95\%\ \text{CL})/\epsilon N_{\text{prod}}\ ,$$

where $N_{\text{obs}}(95\%\ \text{CL})$ is the 95% confidence limit for the number of observed events. In this case $N_{\text{obs}}(95\%$ CL) is 3.0, since no events were observed. In fig. 2a, contours for various limits on Br are given in the $M(\tilde{Z})$–$M(\tilde{e})$ plane for two values of $M(\tilde{\gamma})$. The figures can also be interpreted in the following way: For the branching ratio fixed, say at 10%, the mass region below and at the left of the 10% contour is excluded with 95% CL. For small values of the photino mass and branching ratios greater than 10%, zino masses up to 28 GeV are ruled out if the scalar electron mass is less than 40 GeV.

*Case (B).* $\tilde{Z} \to \mu^+\mu^-\tilde{\gamma}$. The selection criteria for this process are identical to those used in the search for $\tilde{\mu}^+\tilde{\mu}^-$ pair production discussed elsewhere [‡8].

(1) Events were required to have exactly two charged tracks both of which were consistent with muons.

(2) The higher momentum track had to have a momentum greater than 3.5 GeV/$c$ and the lower momen-

[‡7] The lead-glass blocks in the barrel part have, in the $r$–$\varphi$ projection, a width of about 100 mm; the gap between them is about 1.5 mm.

[‡8] For a search for scalar muons, see ref. [16]. For the analysis of the muonic channel for CM energies below 37 GeV a reduced data sample corresponding to 37 pb$^{-1}$ was used since an efficient trigger for such events has been in operation only since 1982. The total luminosity for the analysis of this channel was 48 pb$^{-1}$ ($\sqrt{s}$ up to 45 GeV).

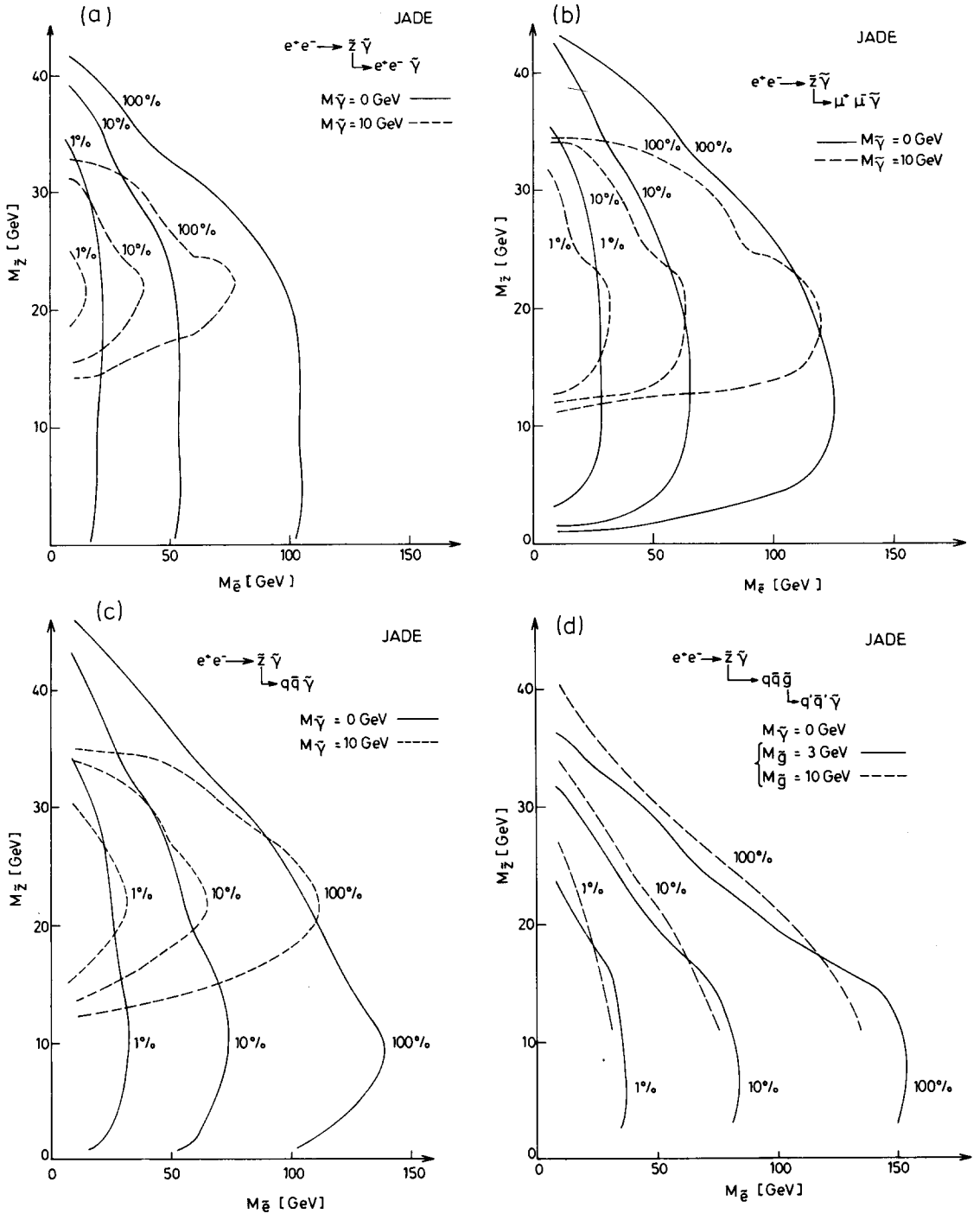


Fig. 2. 95% CL contours defining the excluded regions in the $M(\tilde{Z})$–$M(\tilde{e})$ plane for three values of the branching ratio (1%, 10%, 100%). The region to the left side of the curve is excluded. (a) for $\tilde{Z} \to e^+e^-\tilde{\gamma}$ decay with $M(\tilde{\gamma}) = 0$ GeV (full curve) and $M(\tilde{\gamma}) = 10$ GeV (broken curve). (b) for $\tilde{Z} \to \mu^+\mu^-\tilde{\gamma}$ decay with $M(\tilde{\gamma}) = 0$ GeV (full curve) and $M(\tilde{\gamma}) = 10$ GeV (broken curve). (c) for $\tilde{Z} \to q\bar{q}\tilde{\gamma}$ decay with $M(\tilde{\gamma}) = 0$ GeV (full curve) and $M(\tilde{\gamma}) = 10$ GeV (broken curve). (d) for $\tilde{Z} \to q\bar{q}\tilde{g}$ decay and subsequent decay $\tilde{g} \to q'\bar{q}'\tilde{\gamma}$ with $M(\tilde{g}) = 3$ GeV (full curve) and $M(\tilde{g}) = 10$ GeV (broken curve). For both cases, a massless photino is assumed.

tum had to be greater than 0.2 GeV/$c$.

(3) The acoplanarity angle, defined in the same way as above had to satisfy $20° < \varphi_{\text{acop}} < 150°$.

(4) The missing transverse momentum had to be large, i.e.

$$P_{\text{Tmiss}} = \left[\left(\sum p_{xi}\right)^2 + \left(\sum p_{yi}\right)^2\right]^{1/2} > 3.5 \text{ GeV},$$

where the summation runs over the two charged tracks.

(5) Events were rejected if the missing momentum was pointing to the gap between the barrel and the end cap lead-glass counters.

No events were observed after these cuts. Again the detection efficiency was computed as the function of masses. The detection efficiency is a function of the scalar muon mass as well. For high $\tilde{\mu}$ masses, the decay angular and energy distributions are independent of the $\tilde{\mu}$ mass. For low $\tilde{\mu}$ masses the efficiency depends weakly on the $\tilde{\mu}$ mass. The mode $\tilde{Z} \to \mu\tilde{\mu}$ is also possible in this case. For the mass limit calculations, the conservative approach of choosing the smallest detection efficiency was adopted. For the case of massless photinos, the detection efficiency is about 3% at $M(\tilde{Z}) = 2$ GeV, increases to 50% at $M(\tilde{Z}) = 10$ GeV and reaches the asymptotic value of 65% at $M(\tilde{Z}) = 25$ GeV. It is approximately independent of the $\tilde{e}$ and $\tilde{\mu}$ mass. Upper limits of the branching ratio are then obtained for a given mass combination of $\tilde{Z}$ and $\tilde{\gamma}$, as in case (A). The resulting branching ratio contours in the $M(\tilde{Z})$–$M(\tilde{e})$ plane are shown in fig. 2b, for two values of $M(\tilde{\gamma})$. The contours are quite different from those in fig. 2a because of the different selection criteria. At low $\tilde{e}$ masses, a similar range is excluded for the zino mass.

*Case (C).* $\tilde{Z} \to q\bar{q}\tilde{\gamma}$ *or* $q\bar{q}\tilde{g}$. For the hadronic final states $q\bar{q}\tilde{\gamma}$ and $q\bar{q}\tilde{g}$ only the particles from the hadron jets are observable. Hence the search for these events was made in the multihadron event sample [14] consisting of about 42 000 events with $27 < \sqrt{s} < 37$ GeV and about 6 000 events with 37 GeV $< \sqrt{s} < 46$ GeV. We repeat here the main cuts for their selection:

– Either the shower energy in the lead-glass barrel part had to exceed 3 GeV or each end cap had to contain more than 0.4 GeV.

– At least 4 tracks were required to come from a cylindrical fiducial volume of 30 mm radius and ±350 mm length around the interaction point. Of the tracks, three had to come from the interaction point and had to have transverse momenta greater than 50 MeV/$c$ relative to the beam. $\tau^+\tau^-$ events were suppressed by rejecting four-track events if three of the tracks were in a narrow cone approximately opposite to the fourth track.

We have not applied the cuts on visible energy and longitudinal momentum balance described in ref. [13].

The experimental signature for the hadronic channels depends on the mass of the decaying zino. This is best illustrated for the case $e^+e^- \to \tilde{Z}\tilde{\gamma}_1$ with $\tilde{Z} \to q\bar{q}\tilde{\gamma}_2$. At low zino masses ($\lesssim E_{\text{beam}}$), the hadrons from the q and $\bar{q}$ generally will combine into one jet. The hemisphere opposite to this jet contains the invisible photino $\tilde{\gamma}_1$. Typical events will thus have one jet in one hemisphere, a large missing momentum, and no or few particles in the opposite hemisphere. At high zino mass ($\gtrsim E_{\text{beam}}$), the three-body zino decay will be more isotropic in the lab system and hence the q and $\bar{q}$ jets will normally be separate jets. These jets, however, will be acoplanar with the beam direction. For the decay $\tilde{Z} \to q\bar{q}\tilde{g}$ with $\tilde{g} \to q\bar{q}\tilde{\gamma}$, the topological behaviour as a function of zino mass is qualitatively similar as that for $\tilde{Z} \to q\bar{q}\tilde{\gamma}$. Hence candidate events for both channels were selected using two different selection criteria:

(C1) Selection of single-jet topology.

(1) The polar angle of the event thrust axis had to satisfy $|\cos \vartheta_{\text{th}}| < 0.65$, where $\vartheta_{\text{th}}$ is the polar angle of the event thrust axis relative to the positron beam direction.

(2) The missing transverse momentum $P_{\text{Tmiss}}$ relative to the beam had to exceed 7 GeV.

(3) The plane normal to the thrust axis defines two hemispheres. The total visible energy $E_{\text{back}}$ of all the particles in the backward hemisphere, i.e. opposite to the thrust axis, was required to be small: $E_{\text{back}} < 1$ GeV.

(4) In order to reject $\tau^+\tau^-$ events with very acoplanar charged tracks, no charged tracks at all were allowed in the backward hemisphere, in addition to cut (3).

(5) Cuts (1)–(4) can be satisfied by events with an energetic photon escaping through a gap between the lead-glass blocks thus causing a high $P_{\text{Tmiss}}$. For this reason events were rejected if they failed the following additional requirements:

– The innermost barrel muon chamber exhibited hits within ±10° of the missing transverse momentum direction which were consistent with hits due to an electromagnetic shower.

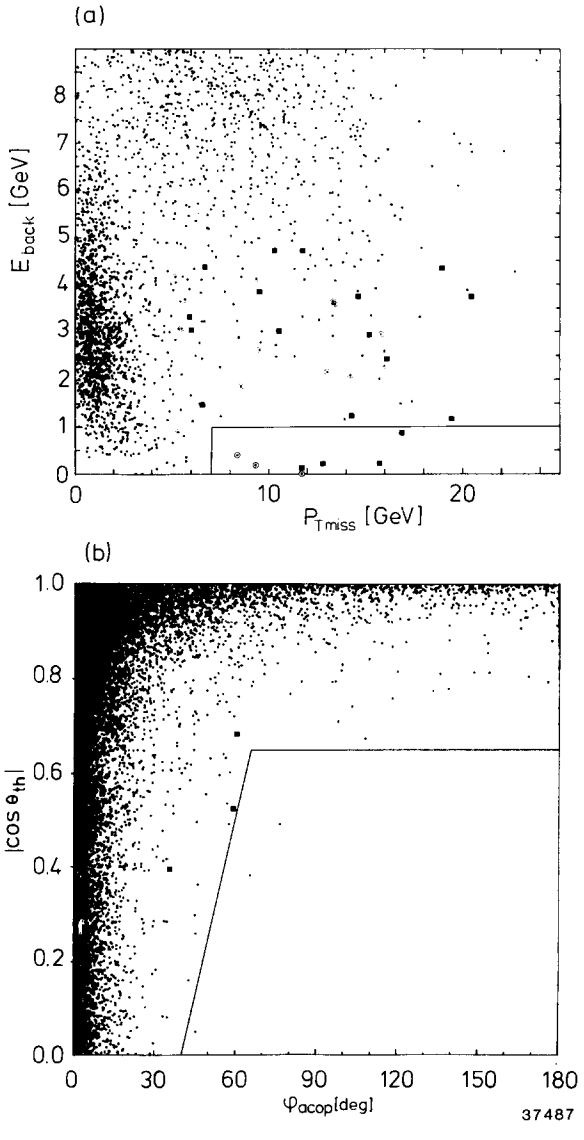


Fig. 3. (a) Scatter plot $E_{\mathbf{back}}$ versus $P_{\mathbf{Tmiss}}$ for the events ($27 < \sqrt{s} < 37$ GeV) passing cut (1) of selection criteria (C1). The final cuts are indicated by full lines. In the region defined by $E_{\mathbf{back}} < 5$ GeV and $P_{\mathbf{Tmiss}} > 5$ GeV, events rejected by cut (4) are represented by the symbol ▪ and those rejected by cut (5) are represented by the symbol ○. (b) Scatter plot $|\cos\vartheta_{\mathbf{th}}|$ versus acoplanarity angle for the events ($27 < \sqrt{s} < 37$ GeV) passing cut (1) of selection (C2). The final cuts are indicated by full lines. Events rejected by cut (4) are shown by the symbol ▪ in the region of $\varphi_{\mathbf{acop}} > 20°\ (1 + |\cos\vartheta_{\mathbf{th}}|)$ and $|\cos\vartheta_{\mathbf{th}}| < 0.7$.

– The forward muon chambers behind the gap between the barrel and endcap lead-glass counters showed hits.
– Runs with the muon chambers not in operation were rejected and the corresponding luminosity was subtracted for the limit calculations.

Fig. 3a shows a scatter plot of $E_{back}$ versus $P_{Tmiss}$ for those events passing cut (1). Cuts (2) and (3) are indicated in the figure. Two photon events populate the region at low $E_{back}$ and low $P_{Tmiss}$, and are effectively removed by cut (2). Multihadron events tend to be located in the region of higher $E_{back}$ (most of them are outside of the plot) and are removed by cut (3). Seven events passed cuts (1), (2) and (3). Of these four events failed cut (4) and the other three events were rejected by cut (5). Thus no events survived the selection criteria (C1).

(C2) Selection of events with acoplanar jets.

(1) The visible energy of the event $E_{vis}$ was required to satisfy $\frac{2}{3}E_{beam} < E_{vis} < 2E_{beam}$, where $E_{vis}$ is obtained by summing up the momenta of the charged tracks and the energies of the lead-glass clusters.

(2) The polar angle of the event thrust axis had to satisfy $|\cos\vartheta_{th}| < 0.65$.

(3) Two hemispheres were defined by the plane perpendicular to the thrust axis. In each hemisphere the particle momenta were summed vectorially. With the two resultant momenta the acoplanarity angle $\varphi_{acop}$ relative to the $e^+e^-$ beam direction was calculated. Only events with large acoplanarity were selected: $\varphi_{acop} > 40° \cdot (1 + |\cos\vartheta_{th}|)$.

(4) After these cuts very acoplanar $\tau^+\tau^-$ events remaining were rejected by the requirement that the number of charged tracks found in each thrust hemisphere was not one.

Fig. 3b shows a scatter plot of $|\cos\vartheta_{th}|$ versus the acoplanarity angle $\varphi_{acop}$ for those events passing cut (1). Cuts (2) and (3) are indicated in the plot. Multihadron events and events due to two-photon processes are located either in the region of small acoplanarity angle or in the region with $|\cos\vartheta_{th}|$ close to unity. The number of events surviving these cuts was zero for $37\ \text{GeV} < \sqrt{s} < 46$ GeV and three for the range $27\ \text{GeV} < \sqrt{s} < 37$ GeV. These three events are characterized by having a rather low visible energy, less than 40% of the CM energy. This makes it most likely that they are due to two-photon processes. This is supported by the fact that one of the events contains a high energy electron candidate. To be on the safe side in obtain-

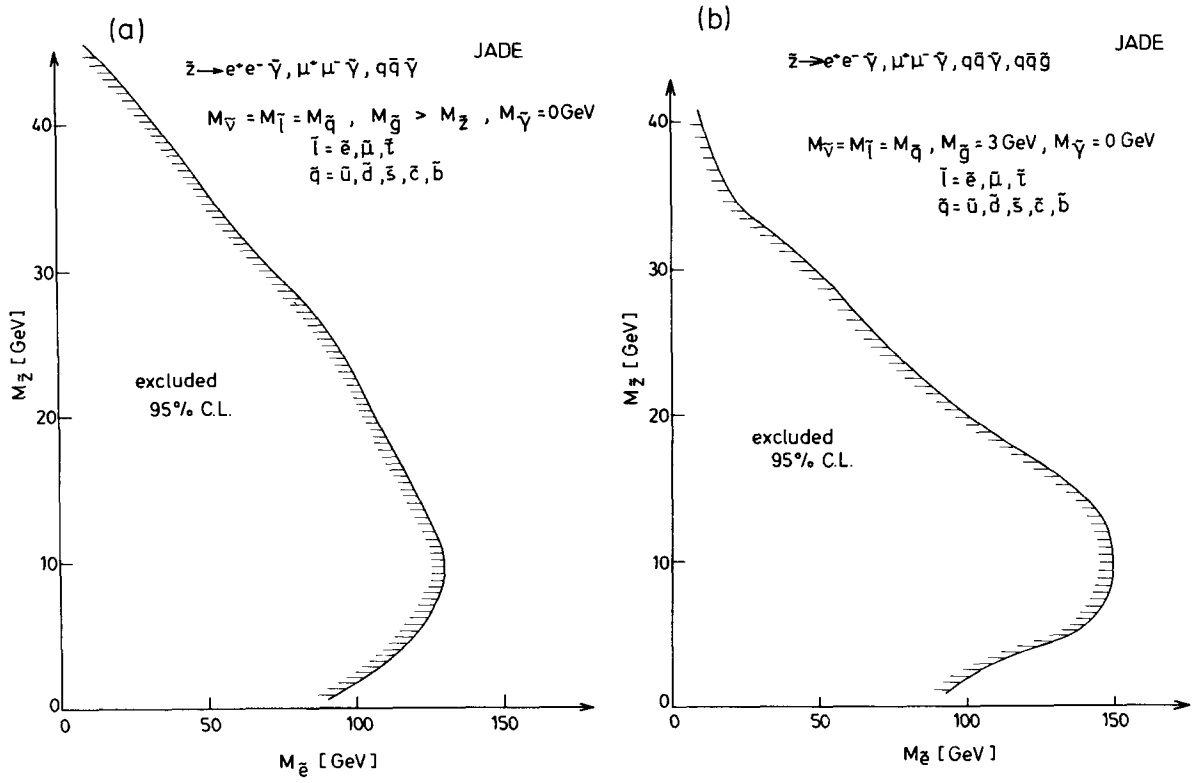


Fig. 4. Excluded region (95% CL) in the $M(\tilde{Z})$–$M(\tilde{e})$ plane. (a) assuming $M(\tilde{\nu}) = M(\tilde{\ell}) = M(\tilde{q})$, $M(\tilde{g}) > M(\tilde{Z})$ and $M(\tilde{\gamma}) = 0$. (b) assuming $M(\tilde{\nu}) = M(\tilde{\ell}) = M(\tilde{q})$, $M(\tilde{g}) = 3$ GeV and $M(\tilde{\gamma}) = 0$.

ing lower limits, these three events were nevertheless kept as candidate events and included in the lower limit calculations.

For both hadronic zino decay modes, the detection efficiency was computed as a function of zino mass, for selection criteria C1 and C2. For the case $\tilde{Z} \to q\bar{q}\tilde{\gamma}$, the efficiency for selection C1 falls from 30–50% at zino masses below $E_{\text{beam}}$ to below 10% at high masses. For selection C2, it rises with increasing zino mass as expected and levels off at about 30% for zino masses larger than $E_{\text{beam}}$. For the case $\tilde{Z} \to q\bar{q}\tilde{g}$, the C1 efficiency is 40–60% at $M(\tilde{Z}) \lesssim E_{\text{beam}}$ and rapidly falls to small values at larger masses. The corresponding C2 efficiency starts at about 45%, falls off less rapidly, however, and exceeds the C1 efficiency at large zino masses. In calculating lower limits for $M(\tilde{Z})$ for a given combination of Br, $M(\tilde{\gamma})$, $M(\tilde{g})$ and $M(\tilde{e})$, that event selection yielding the better limit was chosen. The 95% CL contours in the $M(\tilde{Z})$–$M(\tilde{e})$ plane obtained for the decay mode $\tilde{Z} \to q\bar{q}\tilde{\gamma}$ are shown in fig. 2c for the assignments $M(\tilde{\gamma}) = 0$ and $M(\tilde{\gamma}) = 10$ GeV. As for the leptonic channels the branching ratio $\tilde{Z} \to q\bar{q}\tilde{\gamma}$ has been kept as a free parameter and contours for several values of it are shown. The corresponding curves for the mode $\tilde{Z} \to q\bar{q}\tilde{g}$ are given in fig. 2d. In this case the gluino mass is an additional variable and hence, contours are given for $M(\tilde{\gamma}) = 0$ GeV only, but for two assignments for the gluino mass, namely for $M(\tilde{g}) = 3$ GeV and $M(\tilde{g}) = 10$ GeV.

As stated earlier, the branching ratio is not really a free parameter but can be calculated [17,18] if the masses of the supersymmetric particles are known. In order to get an estimate for the $M(\tilde{Z})$–$M(\tilde{e})$ region allowed by this experiment independent of the branching ratio we made the following working assumption: $M(\tilde{\ell}) = M(\tilde{\nu}) = M(\tilde{q})$. With this the branching ratios were computed and the 95% CL contour in the $M(\tilde{Z})$–$M(\tilde{e})$ plane was determined. This was done for $M(\tilde{\gamma})$

= 0 and for two assignments for the gluino mass: $M(\tilde{g}) > M(\tilde{Z})$ and $M(\tilde{g}) = 3$ GeV. In the first case, the gluino mass was chosen above the zino mass, which suppresses the decay channel $q\bar{q}\tilde{g}$. For zino masses less than the $\tau^+\tau^-\tilde{\gamma}$ threshold, the branching ratios obtained for $e^+e^-\tilde{\gamma}$, $\mu^+\mu^-\tilde{\gamma}$, $\tau^+\tau^-\tilde{\gamma}$ and $q\bar{q}\tilde{\gamma}$ are about 24%, 24%, 0% and 52%, respectively. For zino masses far above the $b\bar{b}\tilde{\gamma}$ threshold, the corresponding values are about 14%, 14%, 14% and 58%, assuming $M(\tilde{e}) > M(\tilde{Z})$. If $M(\tilde{e})$ is smaller than $M(\tilde{Z})$, real scalar leptons or real scalar quarks are produced in the $\tilde{Z}$ decay and the branching ratios for $\nu\tilde{\nu}$, $e\tilde{e}$, $\mu\tilde{\mu}$, $\tau\tilde{\tau}$ and $q\tilde{q}$ are about 38%, 6%, 6%, 6% and 44%, respectively. In the second case ($M(\tilde{g}) = 3$ GeV), the branching ratio for $q\bar{q}\tilde{g}$ is dominant ($\sim$99%), due to the strong coupling constant $\alpha_s$ [+9]. The result of this well defined scenario of supersymmetric masses is shown in figs. 4a, 4b, for the two assumptions of the gluino mass. Only the overall limit obtained by simultaneously combining the results from all four decay channels is given. Zino masses up to about 30 GeV together with scalar electron masses up to 50 GeV are excluded.

In summary, no evidence has been found for single production of the supersymmetric partner of the $Z^0$. The lower limits obtained for the four processes investigated, $e^+e^-\tilde{\gamma}$, $\mu^+\mu^-\tilde{\gamma}$, $q\bar{q}\tilde{\gamma}$ and $q\bar{q}\tilde{g}$ are similar and depend, of course, on the masses of the particles appearing in the final state. For small photino masses, typically lower limits of 30 GeV and 50 GeV can be placed simultaneously on the masses of the zino and the scalar electron, respectively. Smaller zino masses, of the order of 20 GeV, can be excluded together with scalar electron masses as high as 100 GeV.

Thanks are due to O. Nachtmann and A. Reiter for calculating the zino decay matrix elements as well as for several discussions on the theoretical aspects of this work. We also appreciate the advice of T. Sjöstrand about applications of the Lund string model. We are indebted to the PETRA machine group for their excellent support and to all the engineers and technicians who have participated in the construction and maintenance of the apparatus. This experiment was supported by the Bundesministerium für Forschung und Technologie, by the Educational Ministry of Japan and by the UK Science and Engineering Research Council through the Rutherford appleton Laboratory. The visiting groups wish to thank the DESY directorate for the hospitality extended to them.

[+9] The decay channel via the wino, the partner of the W-boson, is neglected because the branching ratio is expected to be very small [17].

*References*

[1] J. Wess and B. Zumino, Nucl. Phys. B70 (1974) 39; Phys. Lett. 49B (1974) 52; A. Salam and B. Strathdee, Phys. Rev. D11 (1975) 1521; P. Fayet and S. Ferrara, Phys. Rep. 32C (1977) 249.
[2] K. Inoue, A. Kakuto, H. Komatsu and S. Takeshita, Prog. Theor. Phys. 67 (1982) 1889; J. Ellis and G.G. Ross, TH.3308-CERN (1982); J. Ellis, J.M. Frere, J. Hagelin, G.L. Kane and S.T. Petcov, SLAC-PUB-3152 (1983).
[3] JADE Collab., D. Cords, Proc. XXth Intern. Conf. on High energy physics (Madison, WI, 1980) p. 595; JADE Collab., S. Komamiya, in: Proc. Workshop on Supersymmetry versus experiment, CERN TH.3311/EP.82/63, p. 57; S. Yamada, in: Proc. Cornell Conf. p. 525; JADE Collab., W. Bartel et al., DESY 84-016 (1984).
[4] S. Weinberg, Phys. Rev. Lett. 50 (1983) 387; P. Fayet, LPTENS 83/16 (1983).
[5] J. Ellis and D.V. Nanopoulos, Phys. Lett. 110B (1982) 44; M. Suzuki, Phys. Lett. 115B (1982) 40.
[6] D.A. Dicus, S. Nandi, W.W. Repko and X. Tata, University of Austin preprint (1983).
[7] JADE Collab., W. Bartel et al., DESY 84-038.
[8] CHARM Collab., F. Bergsma et al., Phys. Lett. 121B (1983) 429; E613 Collab., R.C. Ball et al., UM HE 83-13; UM EX 83-234 (1983).
[9] E. Reya, University of Dortmund preprint, DO-TH 83/17 (1983).
[10] O. Nachtmann and A. Reiter (University of Heidelberg) private communication.
[11] B. Anderson et al., Z. Phys. C1 (1978) 105; B. Anderson and G. Gustafson, Z. Phys. C3 (1980) 223; B. Anderson, G. Gustafson and T. Sjöstrand, Phys. Lett. 94B (1980) 211; T. Sjöstrand, Comput. Phys. Commun. 27 (1982) 243.
[12] JADE Collab., W. Bartel et al., Z. Phys. 20C (1983) 187.
[13] JADE Collab., W. Bartel et al., Phys. Lett. 88B (1979) 175.
[14] JADE Collab., W. Bartel et al., Phys. Lett. 129B (1983) 145.
[15] JADE Collab., W. Bartel et al., in preparation.
[16] JADE Collab., W. Bartel et al., in preparation.
[17] A.H. Chamseddine, P. Nath and R. Arnowit, Phys. Lett. 129B (1983) 445.
[18] M. Glück and E. Reya, University of Dortmund preprint DO-TH 83/24 (1983).